Effect of pseudogap formation on the superconducting gap in underdoped cuprates

E. Schachinger[1,*] and J. P. Carbotte[2,3]
[1]*Institute of Theoretical and Computational Physics, Graz University of Technology, A-8010 Graz, Austria*
[2]*Department of Physics and Astronomy, McMaster University, Hamilton, Ontario, Canada N1G 2W1*
[3]*The Canadian Institute for Advanced Research, Toronto, Ontario, Canada M5G 1Z8*
(Received 30 March 2010; revised manuscript received 11 May 2010; published 24 June 2010)

Many anomalous properties of the normal and superconducting state of underdoped cuprates can be understood qualitatively within a resonating valence bond spin liquid model which incorporates pseudogap formation below a quantum-critical point. It also contains band narrowing, and reduction in coherence, both effects captured through Gutzwiller factors. The superconducting state is treated phenomenologically within the usual BCS model with a *d*-wave superconducting gap. Here we solve a generalized gap equation which explicitly incorporates the emergence of a pseudogap in the electronic structure. The magnitude of the pairing potential is found to still be increasing as the bottom underdoped edge of the superconducting dome is approached. Consequently, it is the Mott physics with implied reduction in metallicity which drives the superconducting critical temperature T_c to zero. The superconducting gap contains many higher harmonics, is nonmonotonic as the magnetic coherence length increases, although its amplitude remains finite everywhere on the Fermi contour even in the antinodal direction where the pseudogap is largest. The superconducting gap to critical temperature ratio increases strongly with decreasing doping.

DOI: 10.1103/PhysRevB.81.214521 PACS number(s): 74.72.−h, 74.20.Mn

I. INTRODUCTION

The superconducting cuprates develop out of an antiferromagnetic Mott insulating state as hole doping (x) is increased away from half-filling. The superconducting critical temperature, $T_c(x)$, as a function of x displays a domelike behavior with $T_c(x)$ decaying on either side of an optimum hole concentration $x=x_{op}$. While overdoped samples have rather ordinary metallic properties, the underdoped region of the phase diagram is anomalous. In particular, a pseudogap[1] develops, one manifestation of which is a general reduction in electronic density of states around the Fermi energy which gets more pronounced with decreasing temperature and doping. The trend toward increasing metallicity with increasing doping x should on its own favor superconductivity so that pairing correlations must, at the same time, decrease as we move to dopings greater than x_{op}. This idea is compatible with a spin-fluctuation pairing mechanism for which the pairing potential is expected to decrease as we move further away from the antiferromagnetic state around $x=0$. The observed *d*-wave gap symmetry is also naturally explained by such a mechanism. Further, one can understand the drop in $T_c(x)$ value in the underdoped regime to be the result of decreasing metallicity as the Mott insulating state is approached, an effect that would need to overcompensate for the increase in spin fluctuations and be able to eventually drive the $T_c(x)$ to zero in the highly underdoped regime.

In this paper we consider the above possibility more critically and base our discussion on the microscopic model developed by Yang *et al.*[2] (YRZ). Their work involves the resonating valence bond (RVB) spin liquid and provides an ansatz for the coherent part of the electronic Green's function which has the very desirable property that it is sufficiently simple, even when generalized to include a superconducting condensation, that it can easily be used to make many predictions based on the model. Calculations have recently shown[3–8] that YRZ provides a semiquantitative understanding of many features previously considered anomalous and, although simplified, captures essential features of the physics of the underdoped regime. The situation is reminiscent of isotropic BCS theory as applied to conventional superconductors. While BCS provides qualitative agreement, for some purposes it is necessary[9–11] to generalize the work to Eliashberg theory which explicitly includes retardation effects associated with the electron-phonon interaction. As an example, BCS predicts universal dimensionless ratios such as twice the gap to k_BT_c to be equal to 3.54. But in some materials the measured values can be quite a lot larger.[9] Of course, retardation effects are also part of the spin-fluctuation exchange theories[12] with *d*-wave gap symmetry. Such effects have not yet been incorporated in the YRZ model which involves an extension of BCS rather than Eliashberg theory. Certainly, inelastic scattering in the cuprates is known to be large and to lead to significant frequency and temperature dependencies in the scattering rates.[13–16] Some attempts to include such effects in the cuprates exist, as one example, in the case of normal-state optical data in Ortho II $YBa_2Cu_3O_{6.5}$, there is an analysis[17] which attempts to incorporate not only retardation but also pseudogap effects, but only at the level of including some reduction in the momentum averaged electronic density of states around the Fermi energy. Such models have proved useful and have provided insight but are much less firmly rooted in microscopic theory than is the model by YRZ. It is not at all clear how such models can be extended to include superconductivity. In conventional metals there are other sources of deviations from isotropic BCS which have been considered. For example, the electron-phonon interaction is very anisotropic[18] and leads directly to large gap anisotropies[19,20] over the Fermi surface. But, again, these are not essential for a first understanding.

Critical elements of the YRZ ansatz are Gutzwiller factors which give the weight remaining in the coherent part of the complete electron Green's function and others which renor-

malize the underlying electronic dispersion curves. These describe the narrowing of the bands as the Mott transition is approached. In addition, below a quantum-critical point (QCP) a pseudogap opens on the antiferromagnetic Brillouin zone (AFBZ). The formulation, while similar to competing order theories[21,22] such as *D*-density waves is quite different in conceptualization. In YRZ the magnitude of the pseudogap increases linearly with decreasing doping x and provides a mechanism for Fermi surface reconstruction. Zero-energy excitations exist only on the contours of the Luttinger pockets. Beyond these there is a finite gap on the momentum contours defined by the energy of minimum approach for the negative energy states which replace the familiar large Fermi surface of ordinary band theory with no pseudogap. The presence of the pseudogap effectively reduces the number of electronic states at and near the Fermi energy. An additional feature of the theory are spectral weights associated with the Fermi contours which can be very different from one and so, not all parts of the Fermi contours will contribute equally to a given phenomenon. As an example, the predicted intensity in an angular-resolved photoemission spectra (ARPES) experiment of the backside of the Luttinger pocket nearest to the antiferromagnetic BZ is weak and has only recently been seen in an experiment.[23] Before only arcs were observed.

To treat the superconducting state, YRZ simply add on to their pseudogap self-energy an additional piece that retains the usual BCS form. This piece is assumed to be unmodified by pseudogap formation although the magnitude of the superconducting gap is treated as phenomenological parameter fixed by the assumption that twice the gap to T_c ratio is six. In this paper we want to examine the validity and/or possible modifications that are required when pseudogap formation is also included in the superconducting gap equation itself. A particular focus is on what impact the existence of a finite normal-state gap on part of the Fermi contour will have on the superconducting gap. To do this we start by writing down a generalized BCS gap equation which incorporates the effect of pseudogap formation on quasiparticle dynamics. For simplicity and to be specific, the pairing potential is taken from the nearly antiferromagnetic Fermi-liquid model[24] (MMP model/form). It describes the exchange of overdamped spin fluctuations and is particularly simple in the static limit.[25–27] It involves two parameters, a coupling constant $[g(x)]$ between the local spin susceptibility and the charge degrees of freedom, and the magnetic coherence length (ξ). The MMP form is retained in most calculations but variations in both magnetic coherence length and coupling $g(x)$ are considered. We also included a few results when an attractive nearest-neighbor pairing interaction is used instead, to provide a comparison. In all cases the coupling $g(x)$ is adjusted to get the measured critical temperature $T_c(x)$ for each x with the magnitude of the pseudogap taken from the theoretical work of YRZ. The resulting gap equation at any temperature below $T<T_c(x)$ is solved using a fast Fourier transform technique.[27,28] Thus, no assumption need be made about the momentum dependence of the resulting superconducting gap solution which is solely determined by the pairing potential and charge carrier dynamics. Our formalism is presented in Sec. II and solutions in Sec. III where the variation in $g(x)$ with doping is given along with the gap to critical temperature ratio, the temperature dependence of the gap amplitude and its dependence on momentum $\mathbf{k}$ in the two-dimensional BZ of the CuO_2 plane. In Sec. IV we present the leading edge gap, or energy of nearest approach, as the Fermi contour is approached. This quantity is just the superconducting gap on the Luttinger pocket around the nodal direction while it is related to an appropriate combination of superconducting gap, pseudogap, and band energies on the remaining part of the Fermi contour around the antinodal direction. We also give more comprehensive results for the changes in the superconducting gap structure in momentum space which results from increasing the magnetic coherence length. The nonmonotonic nature of its variation with angle on the Fermi contours is noted. In particular, its reduction in the antinodal region. In Sec. V we provide a summary of our main results and draw conclusions.

II. FORMALISM

A. Normal state

As a result of complex theoretical considerations based on a RVB spin liquid Yang *et al.*[2] proposed a simple form for the coherent part of the electron Green's function $G(\mathbf{k},\omega,x)$, namely,

$$G(\mathbf{k},\omega,x)=\frac{g_t(x)}{\omega-\epsilon_{\mathbf{k}}(x)-\dfrac{\Delta_{pg}^2(\mathbf{k},x)}{\omega+\epsilon_{\mathbf{k}}^0(x)}}, \tag{1}$$

where $g_t(x)$ is a Gutzwiller factor related to correlations associated with disallowing double occupancy on the same site in the large U limit of the Hubbard model with U the on-site Coulomb repulsion. In Eq. (1), $\mathbf{k}$ is momentum in the two-dimensional BZ of the copper oxide plane with the in plane lattice parameter a. The usual electronic energies are $\epsilon_{\mathbf{k}}(x)$ and $\epsilon_{\mathbf{k}}^0(x)$ is a second energy dispersion which gives the antiferromagnetic BZ boundary for $\epsilon_{\mathbf{k}}^0=0$, which is also referred to as the Umklapp surface. Finally, $\Delta_{pg}(\mathbf{k},x)=\Delta_{pg}^0(x)[\cos(k_xa)-\cos(k_ya)]$ is an input pseudogap calculated by YRZ and given by[6]

$$\Delta_{pg}^0(x)=3t_0(0.2-x) \tag{2}$$

and with d-wave symmetry as a function of momentum $\mathbf{k}$. This input pseudogap is to be distinguished, and differs somewhat, from the pseudogap measured in ARPES as we will describe shortly. The band-structure dispersion curves renormalized by the interactions are given by

$$\epsilon_{\mathbf{k}}(x)=-2t(x)[\cos(k_xa)+\cos(k_ya)]-4t'(x)\cos(k_xa)\cos(k_ya)$$
$$-2t''(x)[\cos(2k_xa)+\cos(2k_ya)]-\mu_p(x) \tag{3}$$

up to third nearest-neighbor hopping with

$$t(x)=g_t(x)t_0+3g_s(x)J\chi/8, \tag{4a}$$

$$t'(x)=g_t(x)t_0', \tag{4b}$$

$$t''(x)=g_t(x)t_0'' \tag{4c}$$

with the Gutzwiller factors given by

$$g_t(x) = \frac{2x}{1+x} \quad \text{and} \quad g_s(x) = \frac{4}{(1+x)^2}. \tag{5}$$

Here, t_0, t_0', and t_0'' are the bare band hopping parameters with $t_0'=-0.3t_0$ and $t_0''=0.2t_0$, J is the magnetic energy of the t-J model taken to be $J=t_0/3$, $\chi=0.338$ is the spin susceptibility, and in much of this work we will take $t_0=175$ meV. The Umklapp surface energy is $\epsilon_{\mathbf{k}}^0=-2t(x)[\cos(k_x a)+\cos(k_y a)]$. Finally, the chemical potential $\mu_p(x)$ is to be determined to get the correct hole doping x based on the Luttinger sum rule. This process was described by Yang *et al.*[2]

Yang *et al.*[5] suggest writing Eq. (1) for the normal state in the form

$$G^N(\mathbf{k},\omega,x) = \sum_{\alpha=\pm} \frac{g_t(x) W_{\mathbf{k}}^{\alpha}(x)}{\omega - E_{\mathbf{k}}^{\alpha}(x)} \tag{6}$$

with

$$E_{\mathbf{k}}^{\pm}(x) = \frac{\epsilon_{\mathbf{k}}(x) - \epsilon_{\mathbf{k}}^0(x)}{2} \pm \sqrt{\left[\frac{\epsilon_{\mathbf{k}}(x) + \epsilon_{\mathbf{k}}^0(x)}{2}\right]^2 + \Delta_{pg}^2(\mathbf{k},x)} \tag{7a}$$

and the Luttinger weights

$$W_{\mathbf{k}}^{\pm}(x) = \frac{1}{2}\left\{1 \pm \left[\frac{\epsilon_{\mathbf{k}}(x) + \epsilon_{\mathbf{k}}^0(x)}{2}\right] \frac{1}{\sqrt{\left[\frac{\epsilon_{\mathbf{k}}(x) + \epsilon_{\mathbf{k}}^0(x)}{2}\right]^2 + \Delta_{pg}^2(\mathbf{k},x)}}\right\}. \tag{7b}$$

It is instructive to consider the normal state in the limit when the pseudogap is set equal to zero. In this limit the Green's function of Eq. (6) should reduce to the ordinary band case possibly modified by Gutzwiller factors if one so wishes. When $\Delta_{pg}^0 \to 0$ in Eqs. (7) we get

$$E_{\mathbf{k}}^{\pm} = \frac{\epsilon_{\mathbf{k}} - \epsilon_{\mathbf{k}}^0}{2} \pm \left|\frac{\epsilon_{\mathbf{k}} + \epsilon_{\mathbf{k}}^0}{2}\right|, \tag{8a}$$

$$W_{\mathbf{k}}^{\pm} = \frac{1}{2}[1 \pm \mathrm{sgn}(\epsilon_{\mathbf{k}} + \epsilon_{\mathbf{k}}^0)], \tag{8b}$$

where $g_t(x)$ was set equal to one. For $\epsilon_{\mathbf{k}}+\epsilon_{\mathbf{k}}^0>0$, $E_{\mathbf{k}}^{+}=\epsilon_{\mathbf{k}}$ with $W_{\mathbf{k}}^{+}=1$ and $E_{\mathbf{k}}^{-}=-\epsilon_{\mathbf{k}}^0$ with $W_{\mathbf{k}}^{-}=0$. On the other hand, if $\epsilon_{\mathbf{k}}+\epsilon_{\mathbf{k}}^0<0$, $E_{\mathbf{k}}^{+}=-\epsilon_{\mathbf{k}}^0$ with $W_{\mathbf{k}}^{+}=0$ and $E_{\mathbf{k}}^{-}=\epsilon_{\mathbf{k}}$ with $W_{\mathbf{k}}^{-}=1$. In both cases the weight $W_{\mathbf{k}}$ is zero for the antiferromagnetic BZ (defined by $\epsilon_{\mathbf{k}}^0=0$) energy $\epsilon_{\mathbf{k}}^0$ which (as it must) drops out of Eq. (6) and $G^N(\mathbf{k},\omega,x)$ reduces to its usual form $1/(\omega-\epsilon_{\mathbf{k}})$. Here, as everywhere else we should really replace ω by $\omega \pm i0^+$ to get the retarded or advanced version of the Green's function.

Pertinent details associated with the Green's function in Eq. (6) are given in Fig. 1 which shows the first quadrant of the first BZ of the CuO_2 plane. For convenience we introduce an angle centered around the M point. The $\overline{\mathrm{MX}}$ line corresponds to $\theta=0°$ and the $\overline{\mathrm{M\Gamma}}$ line to $\theta=45°$. The dashed-dotted (black) line which connects the X with the Y point indicates the AFBZ in this quadrant. The heavy dashed-double dotted (blue) line represents the normal state large Fermi surface defined by band theory as $\epsilon_{\mathbf{k}}=0$ with the dispersion relation $\epsilon_{\mathbf{k}}$ given in Eq. (3) and $t_0=175$ meV. It is for the doping $x=x_{op}=x_{\mathrm{QCP}}=0.2$ which defines the quantum-critical point for which the pseudogap just becomes equal to zero. Zero-energy quasiparticle excitations are possible along this line. In contrast, the heavy solid and dashed (red) lines represent the Fermi contour for doping $x=0.1$ in the heavily underdoped regime where the pseudogap has a rather large amplitude as defined in Eq. (2). This Fermi contour is typical for the Fermi surface reconstruction which results from the opening of a pseudogap in the YRZ model. The Fermi contour is divided into two distinctive regions. One region is called the Luttinger pocket and is presented as the light (blue) shaded area enclosed by the solid and dashed (red) lines. This Luttinger area is a hole pocket. The effective pseudogap is equal to zero on the solid and dashed (red) lines forming its boundary and so represent a true Fermi surface on which zero-energy quasiparticle excitations are possible.

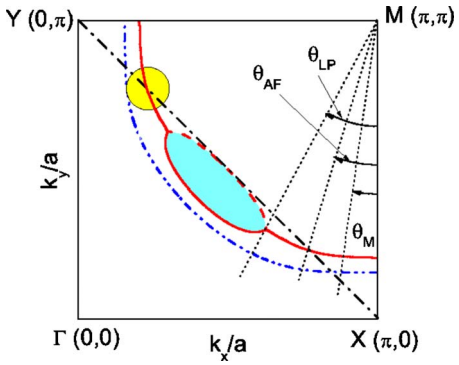

FIG. 1. (Color online) The first quadrant of first Brillouin zone of the CuO_2 plane. The dashed-dotted (black) line which connects the X with the Y points represents the AFBZ in this quadrant. The heavy dashed-double dotted (blue) line is the normal state Fermi surface defined by $\epsilon_{\mathbf{k}}=0$ for doping $x=0.2$ for which the pseudogap is equal to zero. The heavy solid and dashed (red) lines give the Fermi contour for doping $x=0.1$ obtained from consideration of energies of nearest approach associated with $E_{\mathbf{k}}^{-}$.

The equation that defines this contour in $\mathbf{k}$ space is $E_{\mathbf{k}}^{-}(x)=0$ [Eq. (7a)]. The momentum on this curve $\mathbf{k}_{cont}$ can be characterized by its magnitude and an angle θ as in Fig. 1. It is important to note that the Luttinger weight $W_{\mathbf{k}}^{-}$ is of the order one only along the solid (red) line while it is smaller on the backside of the Luttinger pocket [heavy dashed (red) line] which, thus, is not so important in some considerations. Nevertheless, it has recently been seen by Meng *et al.*[23] in an underdoped sample of $Bi_2Sr_{2-x}La_xCuO_{6+\delta}$ with a critical temperature $T_c=18$ K in laser ARPES. The Luttinger pocket is connected to additional Fermi arcs, shown as solid (red) arcs with the border lines MX and MY. These arcs develop out of the continuation of the $E_{\mathbf{k}}^{-}(x)$ branch of the energy spectrum. Along these arcs, however, there is a finite effective pseudogap and, thus, zero-energy quasiparticle excitations are not possible. The arcs are gapped and correspond only to a Fermi contour. For the specific case shown with $x=0.1$ these arcs correspond to the momentum contour where the energy $|E_{\mathbf{k}}^{-}|$ of Eq. (7a) is minimum but not zero. The equation that needs to be solved to get the momentum vector which defines this arc is $|E_{\mathbf{k}}^{-}(x)|=$Min. along the direction θ. For the entire contour we have verified that $E_{\mathbf{k}}^{-}(x)$ is negative and, hence, corresponds to occupied states. Such energies of nearest approach (or leading edge gaps/energies) are measured directly in ARPES experiments[29] and are identified here with the empirical value of an effective pseudogap. There are also energies of nearest approach associated with the $E_{\mathbf{k}}^{+}$ branch of the YRZ spectrum but these energies are large and not zero for angles corresponding to the Luttinger pockets. For all angles θ they define a second momentum space contour that we will describe in detail in Sec. IV. $E_{\mathbf{k}}^{+}(x)$ on this second contour is always positive and, so, is not measured directly in ARPES at $T=0$. The energy of nearest approach along this second arc can be smaller than its value for the same angle $\theta<\theta_{\mathrm{LP}}$ on the $E_{\mathbf{k}}^{-}(x)$ branch. For x approaching x_{QCP} it can even have a region of zeros and a new piece of Fermi surface emerges near the antinodal direction.

For reference in later parts of this paper we introduce besides the angles θ_{LP} which identifies the point in the BZ at which the Luttinger pocket connects to the Fermi arc, θ_{AF} the point in the BZ at which the Fermi contour crosses the AFBZ, and θ_{M} the point on the Fermi contour at which the superconducting gap will have its maximum value, as will be found later. Also, for later reference, the (yellow) shaded circle is meant to represent the range of the MMP form for the pairing potential when transitions through the commensurate magnetic vector $\mathbf{Q}=(\pi,\pi)$ are considered, here shown to be centered around the hot spot for $x=0.1$ defined by the crossing of the Fermi contour with the AFBZ.

B. Superconducting state

In the superconducting state YRZ define the quasiparticle Green's function

$$G^{S}(\mathbf{k},\omega,x)=\sum_{\alpha=\pm}\frac{g_t(x)W_{\mathbf{k}}^{\alpha}(x)}{\omega-E_{\mathbf{k}}^{\alpha}(x)-\dfrac{\Delta_{sc}^{2}(\mathbf{k},x)}{\omega+E_{\mathbf{k}}^{\alpha}(x)}} \tag{9}$$

with the superconducting gap, $\Delta_{sc}(\mathbf{k},x)$. It is taken to have d-wave symmetry (as does the input pseudogap) and to vary with momentum $\mathbf{k}$ in the BZ according to the lowest order harmonic, namely,

$$\Delta_{sc}(\mathbf{k},x)=\Delta_{sc}^{0}(x)[\cos(k_x a)-\cos(k_y a)] \tag{10}$$

with $\Delta_{sc}^{0}(x)$ its amplitude at maximum. The spectral densities associated with the usual and Gor'kov anomalous Green's function which we denote by $A(\mathbf{k},\omega,x)$ and $B(\mathbf{k},\omega,x)$, respectively, are

$$A(\mathbf{k},\omega,x)=g_t(x)\sum_{\alpha=\pm}W_{\mathbf{k}}^{\alpha}(x)\{[u^{\alpha}(x)]^2\delta[\omega-E_{\mathbf{k},S}^{\alpha}(x)]+[v^{\alpha}(x)]^2\delta[\omega+E_{\mathbf{k},S}^{\alpha}(x)]\} \tag{11a}$$

and

$$B(\mathbf{k},\omega,x)=g_t(x)\sum_{\alpha=\pm}\frac{W_{\mathbf{k}}^{\alpha}(x)\Delta_{sc}(\mathbf{k},x)}{2E_{\mathbf{k},S}^{\alpha}}\{\delta[\omega+E_{\mathbf{k},S}^{\alpha}(x)]-\delta[\omega-E_{\mathbf{k},S}^{\alpha}(x)]\} \tag{11b}$$

with $\delta[\cdots]$ Dirac's δ-distribution and

$$[u^{\alpha}(x)]^2=\frac{1}{2}\left[1+\frac{E_{\mathbf{k}}^{\alpha}(x)}{E_{\mathbf{k},S}^{\alpha}(x)}\right], \tag{12a}$$

$$[v^{\alpha}(x)]^2=\frac{1}{2}\left[1-\frac{E_{\mathbf{k}}^{\alpha}(x)}{E_{\mathbf{k},S}^{\alpha}(x)}\right], \tag{12b}$$

$$E_{\mathbf{k},S}^{\alpha}(x)=\sqrt{[E_{\mathbf{k}}^{\alpha}(x)]^2+\Delta_{sc}^{2}(\mathbf{k},x)}. \tag{12c}$$

An important element of YRZ theory is that the application of the above formulas to the calculation of superconducting properties of the underdoped cuprates and comparison with experimental results considered till now anomalous, have provided qualitative and even semiquantitative understanding of this data. To elaborate on a few examples, Valenzuela and Bascones,[3] applied the theory at zero temperature to Raman scattering and found that the observation[30,31] that the energy of the peak in the Raman cross section in B_{2g} symmetry (nodal) moves down while for B_{1g} symmetry (antinodal) it moves up with decreasing doping, could be traced to the increase in pseudogap amplitude while at the same time the superconducting gap decreases. Later work by LeBlanc *et al.*[6] provided understanding of the distinct temperature evolution of the two gap scales extracted from B_{2g} (nodal) and B_{1g} (antinodal) spectra observed by Guyard *et al.*[31,32] The effect on the Raman cross section of the Fermi surface reconstruction which accompanies an increase in pseudogap amplitude as doping is decreased below the quantum-critical point at $x_{\mathrm{QCP}}=0.2$ is discussed and related to the very rapid rise in Raman derived antinodal and nodal gap ratio at a doping somewhat below that of the QCP reported by Guyard *et al.*[31,32] It also provides an explanation for the observed[30] rapid loss in the intensity of the superconducting signal in B_{1g} with decreasing doping while this is not the case in B_{2g}. Specific-heat data by Lorama *et al.*[33] and Loram *et al.*[34] show that the jump at T_c is greatly reduced in magnitude in the deeply underdoped region of the phase diagram and that the electronic specific-heat coefficient γ which is constant in an ordinary Fermi liquid decreases considerably as T is re-

duced toward T_c. In addition, the condensation energy shows an anomalous decrease below its expected BCS value. LeBlanc *et al.*[6] show that all these observations find a natural explanation in YRZ. Yang *et al.*[5] find good agreement with recent ARPES data[35,36] for the variation in the quasiparticle weighting factors $W_{\mathbf{k}}^{\pm}$ and for the corresponding maxima in the energy dispersion. They also can understand the observed particle-hole asymmetry. Carbotte *et al.*[8] considered penetration-depth data. In particular, they can understand the long standing observation that the value of the zero-temperature penetration depth is strongly dependent on doping at the lower end of the superconducting dome while the slope of its linear low T dependence (characteristic of d-wave superconducting gap symmetry) is not. Fermi surface reconstruction and, more importantly, the appearance of the Gutzwiller coherence factors play an essential role in understanding the most recent data[37] of $Bi_2Sr_2CaCu_2O_{8+\delta}$ (Bi2212) and their relationship to the Uemura plot.[38] Understanding of the relationship between the YRZ approach and other prominent theoretical models such as the nodal liquid and Fermi surface arcs[39–41] is also provided in Refs. 6 and 8. Illes *et al.*[4] considered optical properties and were able to understand the two gap scales observed in the missing area under the real part of the optical conductivity as a function of the upper limit on the partial sum of its spectral weight observed by Homes *et al.*[42] Also the prominent "hatlike" structures found in the real part of the optical self-energy[17,43,44] are seen to be part of YRZ theory although another contribution to these hats comes from inelastic scattering[44–46] not included in the calculations. Finally, we mention the work by Bascones and Valenzuela[47] who address the issue of the checkerboard pattern observed in scanning-tunneling microscope spectroscopy (STS) and its relationship to the autocorrelation function associated with photoemission data. It is possible to use the Fourier transform (FT) of the atomic scale spacial inhomogeneities of the STS local density of states (FT-STS) to derive the momentum dependence of the gap. The procedure involves the identification of specific vectors associated with transitions from an octet of regions of high density of states banana-shaped in the quasiparticle contours of constant energy about the Fermi level. Their dependence on energy away from the chemical potential gives the desired gap variation as a function of momentum.[48] We note in passing and we will return to this issue later that the superconducting gap as a function of momentum does not follow a simple lowest harmonic d-wave behavior[48] in such a FT-STS analysis[36,48,49] as is the case in some ARPES measurements.[50] Rather the curve out of the nodal direction shows significant upward behavior. Further discussion on STM and its relation to YRZ is found in Ref. 51.

As outlined above, the YRZ ansatz provides a first understanding of many of the anomalous properties of the superconducting underdoped cuprates which are drastically altered from ordinary BCS behavior. It is important to realize, and as we have already said, that in this formulation, the superconducting gap itself is treated simply as a phenomenological parameter in Eq. (9). The magnitude of its amplitude is fixed from consideration of the observed critical temperature $T_c(x)$ at a given doping x and the assumption that the gap to critical temperature ratio $2\Delta_{sc}(T=0,x)/[k_BT_c(x)]=6$ as some experiments indicate. For its momentum space structure the simplest lowest harmonic form of Eq. (10) is retained and its variation with temperature is assumed to remain BCS mean field. While this is reasonable, it is not at all obvious why the emergence of a pseudogap in the charge dynamics which has drastically modified the properties of this state does not also have a major impact on the superconducting gap itself. For example, on its dependence in $\mathbf{k}$ space, its variation with temperature and on other quantities such as the value of the gap to critical temperature dimensionless ratio. This is the central question we wish to address in this paper. To accomplish this aim we start from a superconducting gap equation generalized to include the emergence of a pseudogap which very significantly alters the electronic structure, as discussed in the previous section, and, consequently, the pairing process.

Within a BCS approach which is sufficient for our purposes here, the pairing potential $V_{\mathbf{k},\mathbf{k}'}$ for scattering from $\mathbf{k}$ to $\mathbf{k}'$ is taken to be instantaneous and frequency independent. The corresponding gap equation takes on the form

$$\Delta_{sc}(\mathbf{k},T,x) = k_BT\frac{1}{\Omega}\sum_{n,\mathbf{k}'} V_{\mathbf{k},\mathbf{k}'}(x)F(\mathbf{k}',i\omega_n,x), \tag{13}$$

where $F(\mathbf{k},i\omega_n,x)$ is the finite-temperature anomalous Gor'kov Green's function with $i\omega_n$ the fermionic Matsubara frequencies and Ω is the volume. $F(\mathbf{k},i\omega_n,x)$ is related in the standard way to the spectral density $B(\mathbf{k},\omega,x)$ given in Eq. (11b). When this expression is substituted into Eq. (13) and the sum over ω_n done we obtain a generalized BCS-type gap equation of the form[52]

$$\Delta_{sc}(\mathbf{k},T,x) = -\sum_{\mathbf{k}',\alpha=\pm} V_{\mathbf{k},\mathbf{k}'}(x)W_{\mathbf{k}'}^{\alpha}(x)\frac{\Delta_{sc}(\mathbf{k}',T,x)}{2E_{\mathbf{k}',S}^{\alpha}(x)}\tanh\left[\frac{E_{\mathbf{k}',S}^{\alpha}(x)}{2T}\right], \tag{14}$$

where T is the temperature and $g_t(x)$ was absorbed into the pairing potential $V_{\mathbf{k},\mathbf{k}'}(x)$. The effect of pseudogap formation is built into the weighting factors $W_{\mathbf{k}}^{\pm}(x)$ in Eq. (14) as well as in the definition of the energies $E_{\mathbf{k},S}^{\pm}(x)$. The linearized in the gap $\Delta_{sc}(\mathbf{k},T,x)$ form of Eq. (14) for $T=T_c$ gives the superconducting critical temperature $T_c(x)$ for a chosen value of x and potential $V_{\mathbf{k},\mathbf{k}'}(x)$. We take the superconducting dome $T_c(x)$ in the underdoped region to be given by

$$T_c(x) = 95.0[1 - 82.6(x-0.2)^2] \tag{15}$$

a relation previously discussed by YRZ. Thus, optimum doping corresponds to $x_{op}=0.2$ with a $T_c=95$ K and this also coincides with the quantum critical point at which the pseudogap begins to be nonzero but these two points could easily be made different[6] although this is of no consequence for the present qualitative discussion.

III. SOLUTIONS OF THE SUPERCONDUCTING GAP EQUATION

A. Nearest-neighbor pairing potential

YRZ assumes that the superconducting gap has a lowest-order harmonic d-wave momentum dependence of Eq. (10). Such a behavior can be simulated in our BCS-type approach using a simple *attractive* nearest-neighbor interaction pairing potential of the form

$$V_{\mathbf{k},\mathbf{k}'}^{(nn)} = -g(x)U_{nn}\{\cos[(k_x - k_x')a] + \cos[(k_y - k_y')a]\}. \tag{16}$$

O'Donovan and Carbotte[26] found that this form leads to solutions of the BCS gap equation which vary in momentum space according to Eq. (10) (lowest d-wave harmonic) for the doping values of interest. In the above $g(x)$ is a coupling parameter which will be determined from the solution of the linearized form of Eq. (14) to give the desired value of $T_c(x)$ in Kelvin on the superconducting dome in Eq. (15). In this regard our approach is different from YRZ who assumed the gap amplitude $\Delta_{sc}^0(x)$ to be determined from the ratio $2\Delta_{sc}^0(x)/[k_B T_c(x)]=6$. Here this ratio is determined by the solution of Eq. (14) at zero temperature and at T_c.

We set $U_{nn}=75$ meV in our model calculations and Fig. 2(a) shows the superconducting dome $T_c(x)$ as solid (black) squares accompanied by the corresponding value of $g(x)$ necessary to find a nontrivial solution of the linearized gap-equation (14) for a given value of $T_c(x)$ on this dome. The coupling parameter $g(x)$ increases monotonically with decreasing doping x which corresponds to an increase in the pseudogap amplitude $\Delta_{pg}^0(x)$. Figure 2(b) gives the maximum of the superconducting gap $\Delta_{\max}(T=0,x)$ at zero temperature [solid (black) up-triangles, left-hand scale applies] and the ratio $2\Delta_{\max}(T=0,x)/[k_B T_c(x)]$ [open (red) squares, right-hand scale applies]. This ratio varies from 4.4 for $x=0.2$, almost the canonical BCS value for d-wave superconductivity, to 8.27 for $x=0.1$, the lowest value of doping investigated. The effect of the pseudogap together with the Fermi surface reconstruction becomes obvious. With decreasing doping a strong relative increase in the superconducting gap is required to allow for the experimental value of $T_c(x)$. Thus, in contrast to YRZ, the superconducting dome for the superconducting gap is different from the superconducting dome described by Eq. (15). If we had not increased the coupling $g(x)$ with decreasing x the superconducting dome in the underdoped regime would have ended at $x\sim 0.12$ rather than below $x=0.1$ as indicated by the dashed (black) line in Fig. 2(a).

Careful evaluation of the momentum dependence of the superconducting gap, i.e., testing for possible contributions beyond Eq. (10) in the superconducting gap, in the whole CuO_2 plane BZ revealed that even at the lowest doping investigated the superconducting gap follows Eq. (10) within numerical accuracy for a potential of form (16). Thus, this simple but, nevertheless, instructive example demonstrates that the pseudogap and the Fermi surface reconstruction which accompanies it, has no effect on the symmetry of the superconducting gap itself. As we will see in the next section, a different form of pairing potential can introduce higher harmonics in the superconducting gap and the pseudogap can enhance these contributions.

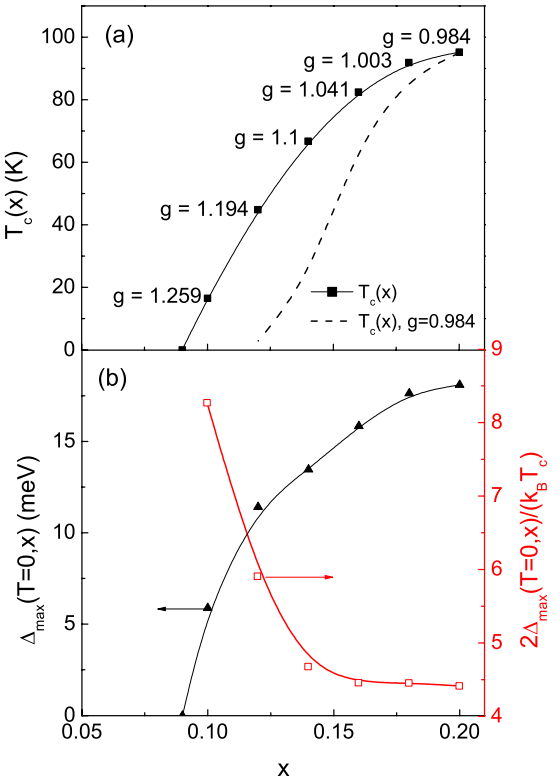

FIG. 2. (Color online) (a) The critical temperature $T_c(x)$ in Kelvin as a function of doping x. The solid (black) line gives the empirical formula (15) and the solid (black) squares correspond to the solutions of the linearized version of the gap-equation (14) with the coupling $g(x)$ adjusted to give the empirical T_c. The dashed (black) curve gives $T_c(x)$ when $g(x)$ is kept fixed at its $x=0.2$ value. (b) The maximum value of the superconducting gap in the BZ $\Delta_{\max}(T=0,x)$ at zero temperature as a function of doping x [solid (black) up-triangles]. Left-hand scale applies. The open (red) squares give the superconducting gap to critical temperature ratio $2\Delta(T=0,x)/[k_B T_c(x)]$ as a function of doping x. Right-hand scale applies.

B. Spin-fluctuation pairing potential

An alternative is to use for the pairing potential the form suggested in the work of Millis *et al.*[24] (MMP form) based on the nearly antiferromagnetic Fermi-liquid model with pairing due to the exchange of overdamped spin fluctuations. The static limit of their pairing potential is particularly simple and sufficient for our approach here which we want to keep as simple as possible. It has the form

$$V_{\mathbf{k},\mathbf{k}'}(x) = g(x)\frac{\chi(\mathbf{Q})}{1+\xi^2|\mathbf{k}-\mathbf{k}'-\mathbf{Q}|^2} \tag{17}$$

with the antiferromagnetic commensurate wave vector $\mathbf{Q}$ taken to be (π,π) and symmetry related points. $\chi(\mathbf{Q})$ is the static spin susceptibility which is set to 10 states/eV and $g(x)$ is the coupling constant taken to absorb the Gutzwiller fac-

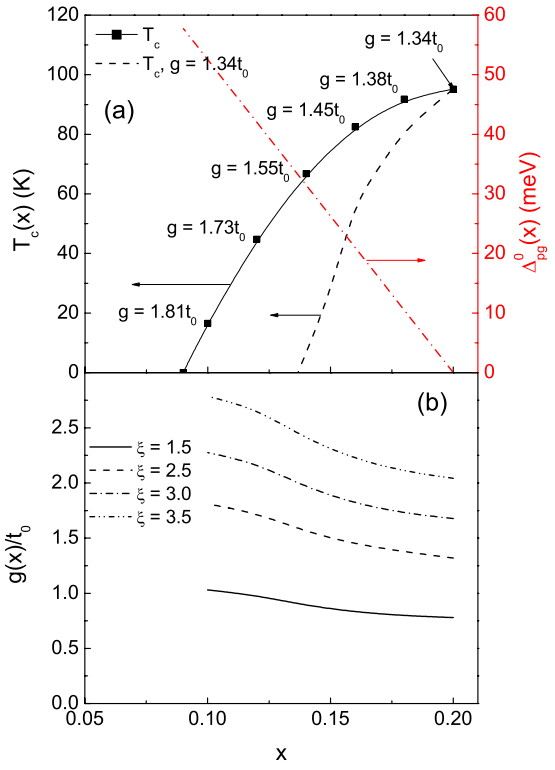

FIG. 3. (Color online) (a) The critical temperature $T_c(x)$ in Kelvin as a function of doping x. As in the work of YRZ we have taken optimum doping to fall at $x=0.2$ which is where the pseudogap opens at a quantum-critical point. The solid (black) line gives the empirical formula (15) and the solid (black) squares are the results of our gap-equation (14) solutions with the coupling $g(x)/t_0$ adjusted to get the empirical T_c. The dashed (black) curve gives results when $g(x)/t_0$ is kept fixed at its $x=0.2$ value. (Left-hand scale) The dashed-dotted (red) line (right-hand scale) gives the pseudogap amplitude according to Eq. (2). (b) $g(x)/t_0$ vs doping x for different values of the magnetic coherence length ξ.

tor. Finally, the magnetic coherence length ξ is set at 2.5 in units of the in-plane lattice parameter a unless otherwise stated. This completely defines our gap-equation (14), with the coupling $g(x)$ calculated from the solution of its linearized version to give the critical temperature $T_c(x)$ according to Eq. (15). The characteristic form in Eq. (17) which we use for the pairing, could, in reality, be more complicated. For example, it could be modified by the emergence of the pseudogap. Here such possible modifications are modeled only by changing the value of the two parameters, the coupling $g(x)$ and the magnetic coherence length ξ which we would expect to increase as the doping is reduced and the antiferromagnetic state is approached more closely. To keep things simple no modification of the functional form of Eq. (17) is introduced.

In Fig. 3(a) we show our results for the superconducting critical temperature $T_c(x)$ in Kelvin as a function of doping x. As we did in the previous section, at each point [solid (black) squares] the coupling $g(x)$ in units of t_0 was recalculated to get the measured T_c for that particular hole doping x given by Eq. (15). It is an important result that, once again, we find it necessary to increase $g(x)$ with decreasing x from $1.34t_0$ at optimum doping ($x=0.2$) where there is no pseudogap and the ordinary large Fermi surface of band theory applies, to $1.8t_0$ at $x=0.1$. If we had not increased the coupling to the spin fluctuations with decreasing x the superconducting dome in the underdoped regime would have ended at $x \sim 0.14$ rather than below $x=0.1$ as indicated by the dashed (black) line. The picture that emerges from these results is that the formation of the pseudogap itself reduces the ability of the charge carriers to effectively pair, a feature consistent with the general expectation that the approach to the Mott insulating state reduces the metallicity of the system. To get the measured value of T_c, the size of $g(x)$ needs to be increased and this is consistent with an increase in magnetic effects as the antiferromagnetic state is approached more. This central result remains even when different values for the magnetic coherence length ξ are used as shown in Fig. 3(b). Four values are considered $\xi=1.5$ (solid curve), $\xi=2.5$ (dashed curve), $\xi=3.0$ (dashed-dotted curve), and $\xi=3.5$ (dashed-double dotted curve). As ξ is increased the variation in $g(x)$ with doping x also increases but even for the smallest ξ considered, there is significant enhancement of the coupling as the antiferromagnetic state is approached. To include such an effect means that in Fig. 3(b) we might want to slide from the dashed curve which applies to $\xi=2.5$, a value taken as characteristic of optimum doping (at $x=0.2$ in this work), to the dashed-double dotted line with $\xi=3.5$ as x is decreased below ($x=x_{\mathrm{QCP}}$). Later we will consider the effect of increasing ξ even more and report explicitly on the case $\xi=10$. As ξ gets very large the form (17) for the pairing potential becomes progressively more peaked about the commensurate magnetic wave vector $\mathbf{Q}$ as a function of momentum transfer $\mathbf{q} \equiv \mathbf{k}' - \mathbf{k}$. In the limit $\xi \to \infty$ which is of course unrealistic for the superconducting cuprates, the pairing becomes $\sim g(x)\chi(\mathbf{Q})/(\pi\xi)$ multiplied by a δ-distribution. We see from this simple formula that the effective coupling must increase to compensate for the factor ξ which appears in the denominator.

An additional important question is how radically does the existence of the pseudogap changes the properties of the superconducting gap itself. This is addressed in the next several figures. In Fig. 4(a) we show results for the zero-temperature superconducting gap to critical temperature ratio $2\Delta_{sc}(0,x)/(k_B T_c)$ as a function of doping x. In our model calculations the gap is defined over the entire Brillouin zone as a function of momentum $\mathbf{k}$. Thus the maximum gap value in the BZ $\Delta_{\max}(0,x)$ need not be the same as its maximum value on the Fermi contour, $\Delta_{\text{FS-max}}(0,x)$. The solid up-triangles are the results when the entire BZ is considered while the solid down-triangles are for the Fermi contour and, as we would have expected, these values are always the smaller of the two. This also holds for the next-nearest-neighbor model. We note that both these ratios vary with x and neither is fixed at the known BCS d-wave value of 4.3. It can be as small as ~ 4.0 and as large as 6.5 with the strongest increase for x below $\lesssim 0.12$. More specifically, for the up-triangles which represent the maximum gap in the BZ it is ~ 6.5 for $x=0.1$ while for the down-triangles (the maximum gap along the Fermi surface) it is ~ 6.15. Both these values are smaller than that found for the nearest-neighbor pairing of the previous section. The corresponding values of the

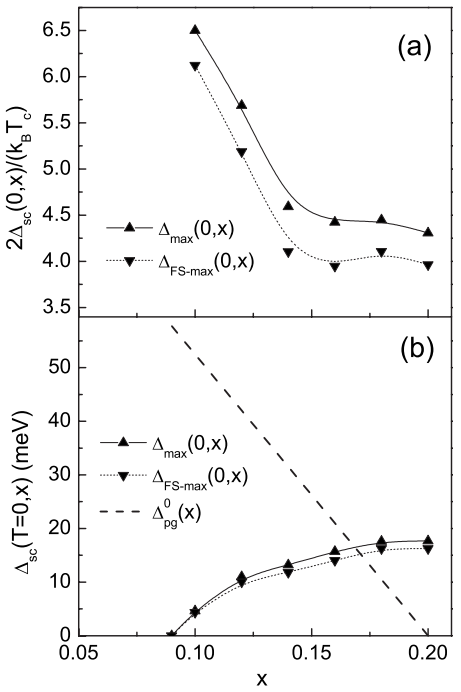

FIG. 4. (a) The zero-temperature gap to critical-temperature ratio $2\Delta_{sc}(0,x)/(k_BT_c)$ as a function of doping x. The solid up-triangles give the maximum gap $T=0$ value $\Delta_{\max}(0,x)$ in the BZ and the solid down-triangles correspond to the maximum gap value $\Delta_{\text{FS-max}}(0,x)$ on the Fermi surface. (b) Compares the maximum gap value in the Brillouin zone (solid up-triangles) and the maximum gap value on the Fermi surface (solid down-triangles) with the amplitude of the pseudogap $\Delta^0_{pg}(x)$ (dashed line) according to Eq. (2).

zero-temperature gaps are given in Fig. 4(b) in which they are also compared with the input pseudogap amplitude $\Delta^0_{pg}(x)$ (dashed line). We stress again that the superconducting dome for the gap does not follow exactly that for $T_c(x)$ of Fig. 3(a) because the gap to critical-temperature ratio in our work is determined by the solution of the gap equation and varies from its classical d-wave value. The change with x in the gap to T_c ratio reported here has its origin in the momentum space behavior of the pairing potential and in the effect of the pseudogap. This is different from what is the case in conventional superconductors where such deviations are often related to retardation effects[9,10] in the pairing which has its origin in the electron-phonon interaction and Eliashberg theory.

In this paper we will treat only the pairing potential which comes from the exchange of spin fluctuations. There is evidence for an additional small contribution due to electron-phonon interaction. A contribution from this mechanism at the level of a $\sim$10% effect was found[53] to be able to explain the shift in "kink" structure seen in the renormalized ARPES dispersion curves in Bi2212 on oxygen isotope substitution $^{16}\text{O}\rightarrow{}^{18}\text{O}$. Also, it is well established that energy dependence in the electronic density of states[54] can significantly enhance the effect of a small phonon contribution on the critical-temperature isotope effect. In particular, the growth of a pseudogap[55] can lead to a large isotope effect for T_c even when the phonons contribute little to the pairing.

Another quantity of interest is the temperature dependence of the superconducting gap. Its root-mean-square

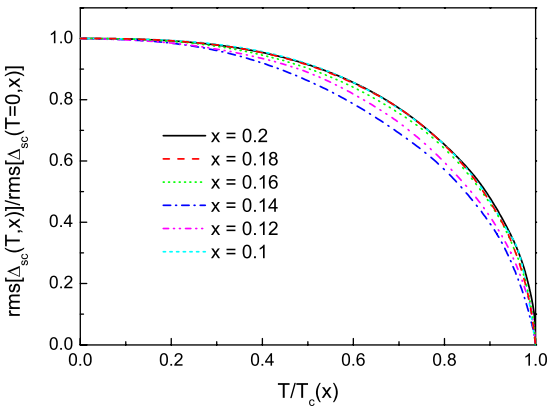

FIG. 5. (Color online) Temperature dependence of the root mean square $\text{rms}[\Delta_{sc}(T,x)]$ at finite T normalized to its value at zero temperature as a function of the reduced temperature $T/T_c(x)$ for various values of the doping parameter x.

(rms) value $\text{rms}[\Delta_{sc}(T,x)]$ at finite T normalized to its value at $T=0$ is given in Fig. 5 as a function of the reduced temperature $T/T_c(x)$ for six values of doping as labeled. The solid (black) curve is for $x=0.2$ which is a case with no pseudogap in our model and here involves the large Fermi surface of band theory. The other cases fall slightly below the solid (black) curve but the trend with decreasing x is not monotonic. First the normalized gap at intermediate reduced temperature $T/T_c(x)$, say 0.7 for definiteness, shows a decrease with decreasing doping. The greatest reduction is reached for $x=0.14$ [dashed-dotted (blue) line] after which it starts to increase again with the case $x=0.1$ [short dashed (cyan) line] close to the $x=0.2$ case. These differences are, however, never large and justify the use of a BCS temperature variation in previous papers[6–8] for the superconducting gap even when there is a large pseudogap present.

Details about the momentum dependence of the superconducting gap and the modifications brought about by the opening of a pseudogap are given in Fig. 6 as contour plots [light solid (black) lines] which are restricted to the first quadrant of the two dimensional CuO_2 BZ. The Fermi contours coming from $E^-_{\mathbf{k}}(x)$ are represented by heavy solid and dashed (white) lines. The figure has four frames for $x=0.2$, $x=0.16$, $x=0.1$, and $x=0.12$ arranged clockwise from the top-left-hand corner. Comparing the cases with $x=0.2$ and $x=0.1$ we see considerable changes in the shape of the constant superconducting gap contours as we enter the underdoped region of the phase diagram. While the case $x=0.2$ is not so different from a simple $[\cos(k_xa)-\cos(k_ya)]$ dependence of ordinary d-wave BCS theory, higher harmonics are present even in this instance as is known from previous work.[25–28] As the value of the pseudogap amplitude is increased there are large changes in the shape of the gap contours, and the contribution from higher harmonics to the superconducting gap function become more important. It is the form of the pairing potential given in Eq. (17) which determines the admixture of higher d-wave harmonics that enter the superconducting gap while this effect is enhanced by the pseudogap. Note, that here we used fast Fourier transforms to solve Eq. (14) and did not need to make any explicit assumption as to the harmonic content of $\Delta_{sc}(\mathbf{k},T=0,x)$. Re-

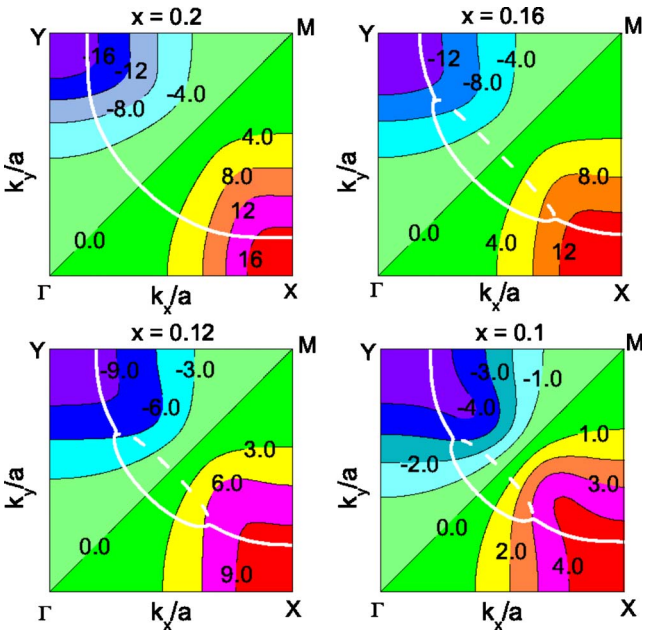

FIG. 6. (Color online) Contour diagram of the superconducting gap as a function of momentum **k** in the first quadrant of the two-dimensional CuO_2 BZ [light solid (black) lines labeled with the actual value of the gap in meV]. The four frames are arranged clockwise for the doping parameters $x=0.2$, $x=0.16$, $x=0.1$, and $x=0.12$. The heavy solid and dashed (white) lines indicate the contour of the Fermi surface as a function of momentum **k** that are determined from energies of nearest approach associated with $E_{\mathbf{k}}^{-}$.

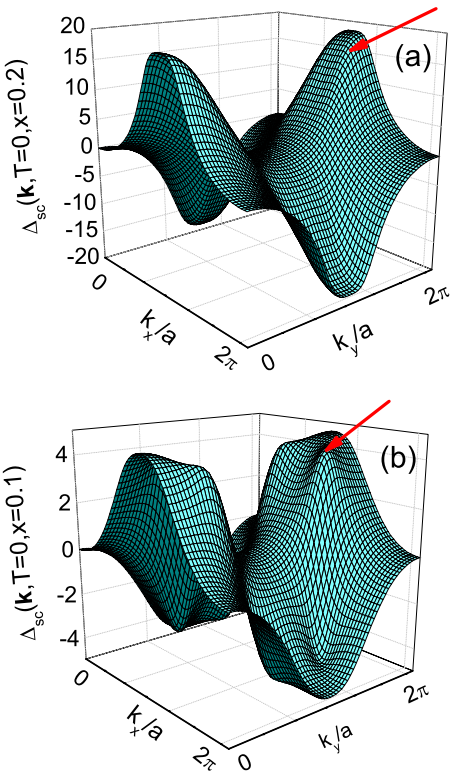

FIG. 7. (Color online) (a) Surface plot of the superconducting gap $\Delta_{sc}(\mathbf{k},T,x)$ for $T=0$ and $x=0.2$ as a function of momentum **k** in the first Brillouin zone of the CuO_2 plane. (b) The same as (a) but for $x=0.1$.

turning to the Fermi contours we note their evolution from a large Fermi contour at $x=0.2$ to the Luttinger pockets in the other three considered which are indicated by the heavy solid and dashed (white) lines. As described in Sec. II A, they are calculated in the normal state and are curves defined in momentum space by the energy of nearest approach (NA) measured in ARPES.

More details concerning the variation in the gaps with momentum **k** that result from our numerical solutions of the generalized gap-equation (14) with the simple static pairing potential in Eq. (17) are shown in Fig. 7(a) for $x=0.2$ and Fig. 7(b) for $x=0.1$. In both cases $T=0$ and the magnetic coherence length ξ in Eq. (17) is fixed to the value of 2.5. These two gap surfaces as a function of **k** are significantly different from each other and are both different from the form $[\cos(k_x a)-\cos(k_y a)]$ although this is not so easily seen for $x=0.2$. When there is a large pseudogap as in Fig. 7(b) a feature which can barely be seen in Fig. 7(a) and which is located by a heavy (red) arrow becomes enhanced and emergence as a peak, again indicated by a heavy (red) arrow, in the top-right-hand part of this figure. These peaks do not necessarily fall on the Fermi contours (Fig. 1) as we have already noted in Fig. 4(b) where, for the case of the magnetic coherence length $\xi=2.5$ the maximum gap on the Fermi contour (solid down-triangles) is always smaller than the maximum gap in the BZ (solid up-triangles). In this case these effects are not large but we will see later when we consider larger values of ξ that they can be greatly enhanced.

IV. ARCS AND ENERGY OF NEAREST APPROACH ON THE FERMI CONTOUR

A question that immediately arises is, how does the superconducting gap which comes from the numerical solution of our modified BCS Eq. (14), vary on the Fermi contour. A direction on this contour can be specified by an angle θ already introduced in Fig. 1 and which is, again, defined in the inset of Fig. 8(a). Figure 8 presents the variation in the superconducting gap as a function of the angle θ on the nearest approach contours determined from $E_{\mathbf{k}}^{-}(x)$ in the normal state. We show four values of doping, namely, $x=0.2$, 0.16, 0.12, and 0.1 and several temperatures as indicated. The solid (black) curve in Fig. 8(a) is for $T=0$ and we see that it is quite different from a pure $\cos(2\theta)$ [dashed (black) curve] variation that has often been assumed to hold. The concave upward behavior of this curve is in qualitative agreement with some ARPES (Ref. 50) as well as with some STS experiments[36,48,49] although in that case the experimental technique of Fourier transforming the spatially varying local density of states does not provide access to data very near the node. The dashed-dotted (red) curve shows that at $T=80$ K the θ dependence of the solutions of the BCS Eq. (14) is again quite different from a simple $\cos(2\theta)$ [dashed-double dotted (red) line]. This is a case of zero pseudogap. The curves for $\Delta_{sc}(T,\theta)$ vs θ in Fig. 8(b) are for $x=0.16$ with a significant input pseudogap the magnitude of which is comparable to the magnitude of the amplitude of the superconducting gap, yet concave upward behavior is still seen. As

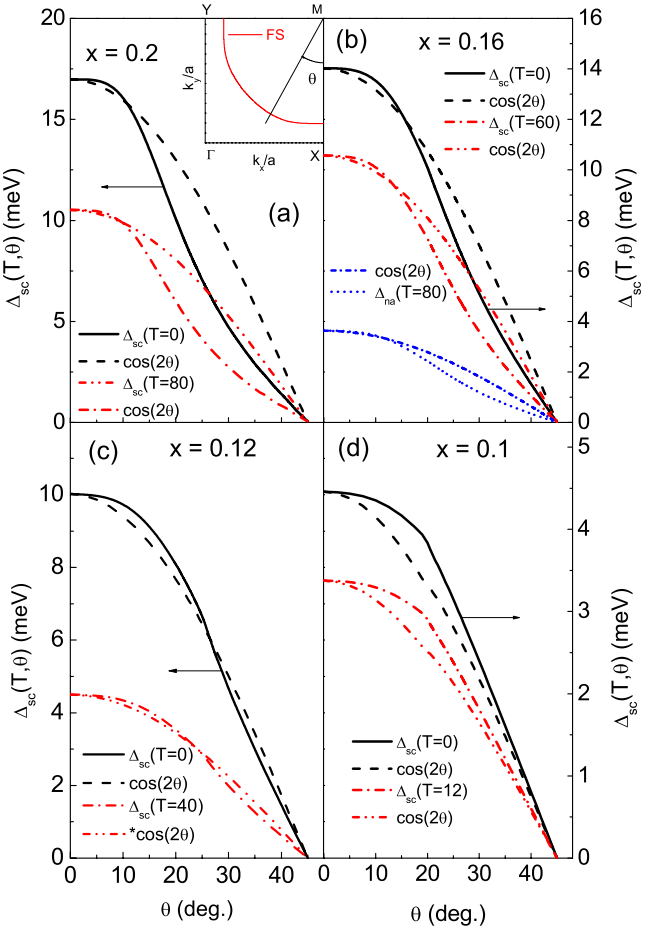

FIG. 8. (Color online) The superconducting gap along the Fermi contour [solid (red) line in the inset] as a function of θ for $x=0.2$ when there is no pseudogap. The solid (black) line gives the zero-temperature solution of Eq. (14) which is compared with the simple d-wave symmetry $\sim \cos(2\theta)$ (dashed line). The (red) dashed-dotted and dashed-double dotted lines give the same results but for $T=80$ K. The inset defines the angle θ within the first quadrant of the two-dimensional Brillouin zone of the CuO_2 plane. The nodal direction (ΓM line) corresponds to $\theta=\pi/4$ while the antinodal direction (XM line) corresponds to $\theta=0$. Frames (b)–(d) are for $x=0.16$, 0.12, and 0.1, respectively, with temperatures as labeled.

we go to even larger values of the input pseudogap amplitude and it becomes much larger than Δ_{sc}, the superconducting gap variation becomes more cosine like, as can be seen in Fig. 8(d), on comparing the solid (black) curve for $T=0$ and dashed-dotted (red) curve for $T=12$ K with dashed (black) and dashed-double dotted (red) curves, respectively. This trend from concave up to more linear variation out of the node as doping is decreased is confirmed by the data of Kohsaka *et al.*[36] We also made comparison (not shown here) with the case of the lowest d-wave harmonic $\Delta_{sc}(\mathbf{k}) \sim [\cos(k_x a)-\cos(k_y a)]$ which is evaluated on the Fermi contour and these are close to the pure $\cos(2\theta)$ curves. Thus, the differences between solid and dashed (black) curves in Fig. 8(d) represent a mixture of higher d-wave harmonics in the solution of Eq. (14) for the superconducting gap. Note the shoulder and a small kink at intermediate θ after which the rate of increase in the gap with decreasing θ toward the antinode is reduced from its relatively much more rapid near linear variation out of the node at $\theta=45°$. In summary, our gap solutions projected on the Fermi contour do not follow the often used $\cos(2\theta)$ form and the deviations found agree with some experiments.[36,50] The differences found are not very large and in that sense provide support for the usual ansatz that Δ_{sc} follows Eq. (10) when the aim is a first qualitative understanding. This result was unexpected. As we have documented at length in Sec. II B pseudogap formation leads to large modifications of superconducting properties, yet we find that its influence on the superconducting gap itself is rather modest.

ARPES gives the superconducting gap directly only on the boundaries of the Luttinger pocket where the pseudogap is zero. On the remainder of the Fermi contour it is a combination of superconducting and empirical pseudogap that is measured. Such curves are presented in Fig. 9 for two dopings, namely, $x=0.12$ in Fig. 9(b) and $x=0.16$ in Fig. 9(a). These curves involve the solution of the gap-equation (14) and the evaluation of the energy $E^{-}_{\mathbf{k},S}(x)$ of Eq. (12c) with $E^{-}_{\mathbf{k}}(x)$ defined in Eq. (7a) and momentum $\mathbf{k}$ on the Fermi contour [heavy solid (white) curves in Fig. 6]. Only the part of the Luttinger pocket with $W^{-}_{\mathbf{k}}$ of order one is shown as in most experiments this is the only piece considered. The energy of nearest approach $\Delta_{\mathrm{NA}}(T,\theta)$ is shown for $T=0$ [solid (black) line], $T=40$ K [dashed-dotted (red) line]. We have introduced temperature only in as much as it modifies the superconducting gap which is the finite temperature solution of Eq. (14) so that the $T=T_c$ curve is the zero temperature normal state case but with finite pseudogap. This effective pseudogap is nonzero only for angles less than θ_{LP} defined in Fig. 1 which range from $\sim 25°$ ($x=0.12$) to $\sim 19°$ ($x=0.16$). In this regard we emphasize that the input pseudogap of Eq. (2) has a finite amplitude for all momenta in the BZ except for the zeros required to preserve d-wave symmetry. On the other hand, the effective pseudogap $\Delta_{\mathrm{NA}}(T,\theta)$ defined by the double-dotted (blue) curve in Fig. 9 is what is measured and this energy is zero on the entire Luttinger contour. Thus, the effective pseudogap $\Delta_{\mathrm{NA}}(T,\theta)$ is clearly not the input pseudogap of YRZ itself although is related to it. In particular, at $\theta=0$ $\Delta_{\mathrm{NA}}(T=0,\theta=0)/t_0 \simeq 0.27$ while $\Delta_{pg}(\theta=0)/t_0 \simeq 0.24$. To be very explicit on this point the input pseudogap $\Delta_{pg}(\mathbf{k},x)=\Delta^0_{pg}[\cos(k_x a)-\cos(k_y a)]/2$ is not zero on the Luttinger contour while $\Delta_{\mathrm{NA}}(T,\theta,x)$ is exactly zero all along this contour. In Eq. (7a) for the energies $E^{\pm}_{\mathbf{k}}(x)$ it is not just the input $\Delta_{pg}(\mathbf{k},x)$ which enters but also $\epsilon_{\mathbf{k}}$ and $\epsilon^0_{\mathbf{k}}$ evaluated on the Fermi contour play a role. For $x=0.12$ [Fig. 9(b)] the finite value of the superconducting gap at $\theta=0$ is responsible for a slight increase in $\Delta_{\mathrm{NA}}(T,\theta=0)$ as T goes to zero. In the ARPES data by Kondo *et al.*[29] no such temperature dependence is observed in their underdoped sample. This is in reasonable agreement with our results. But no temperature variation is also observed at optimum doping while here we find a significant dependence even for $x=0.16$ as shown in Fig. 9(a), which represents a case where the superconducting and pseudogap energy scale are more equal in value. While the nodal direction provides a measure of the superconducting gap alone for $\theta > \theta_{\mathrm{LP}}$, the empirical pseudogap dominates the behavior of this curve at values of θ around the antinodal direction. But still, there remains noticeable temperature de-

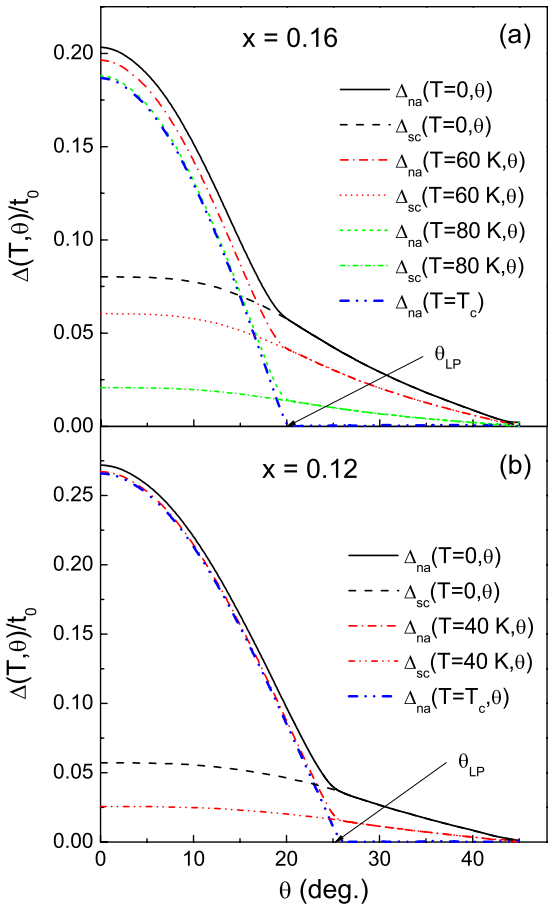

FIG. 9. (Color online) (a) The normalized energy of nearest approach $\Delta_{NA}(T,\theta)/t_0$ for various temperatures as indicated and for doping $x=0.16$ as a function of θ along the Fermi contour [solid (white) line in the top-right frame of Fig. 6]. We also show, for comparison the normalized superconducting gap $\Delta_{sc}(T,\theta)/t_0$. For angles $\theta > \theta_{LP}$ the energies of nearest approach correspond to the superconducting gap because the effective pseudogap is zero on this part of the Fermi contour along the Luttinger pocket. The case $\Delta_{NA}(T=T_c)/t_0$ corresponds to the normal pseudogap state. (b) The same as (a) but now for $x=0.12$. The relevant Fermi contour is found as the solid (white) contour in the left-hand bottom frame of Fig. 6.

pendence at $\theta=0$ which reflects the smaller contribution of the superconducting gap. This fact does not agree with a possible interpretation of the data by Kondo *et al.*[29] in terms of a superconducting gap largely confined to the Luttinger pocket and small or vanishing[7] outside where it competes with the effective pseudogap. Except for the temperature dependence just noted, many other features of these curves are in qualitative agreement with ARPES data[29] which is also confirmed in some recent STS data on the underdoped cuprates.[56] The energy of nearest approach given in Fig. 9 clearly shows two energy gap scales as does the data of Kondo *et al.*[29] There is, however, other ARPES data by Chatterjee *et al.*[57] on Bi2212 which shows a single *d*-wave gap even for dopings beyond the bottom of the superconducting dome which is achieved by using thin films. Such data is interpreted as more consistent with a preformed pair scenario[58,59] than with competing order theories. The source

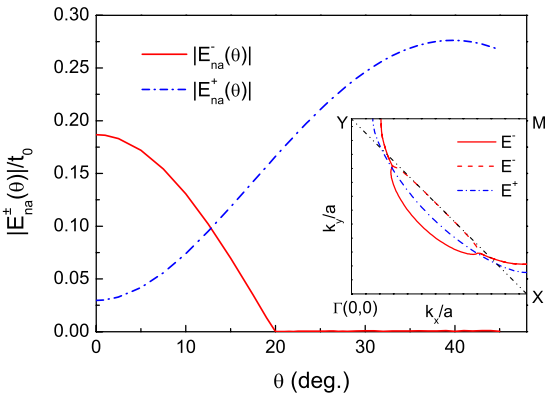

FIG. 10. (Color online) The energies of nearest approach $|E^{\pm}_{NA}|$ as a function of angle θ as defined in Fig. 1 for $x=0.16$. The inset shows the Fermi contours associated with the two energies $E^{\pm}_{\mathbf{k}}$ of the YRZ spectrum in the first quadrant of the CuO_2 Brillouin zone.

of discrepancy between the data is as yet unresolved but could be related to sample preparation.

ARPES traces the contours of minimum approach associated with the $E^-_{\mathbf{k}}$ branch of the YRZ spectrum and it is this branch which gives the Luttinger surfaces on which there is no gap in the normal state. But there are also energies of nearest approach associated with the $E^+_{\mathbf{k}}$ branch and these are shown as the dashed-dotted (blue) curve in Fig. 10 where we compare the results for $|E^-_{\mathbf{k}}|$ [solid (red) curve] for $x=0.16$ and $T=T_c$, i.e., normal pseudogap state, no superconductivity. For angles θ larger that $20°$ $|E^+_{NA}(\theta)|$ is large while $|E^-_{NA}(\theta)|$ is zero. For $\theta<20°$, however, the solid (red) and the dashed-dotted (blue) curve cross and in the antinodal direction $(\theta=0)|E^+_{NA}(\theta=0)|$ is the smallest of the two energies. Note, however, that $E^-_{NA}(\theta)\leq 0$ and $E^+_{NA}(\theta)\geq 0$ for all θ and, thus $E^+_{NA}(\theta) > E^-_{NA}(\theta)$ for all angles θ. The momentum contour of nearest approach associated with $E^+_{NA}(\theta)$ is shown as the dashed-dotted (blue) curve in the inset of Fig. 10 where it is compared to the contours from $E^-_{NA}(\theta)$ [solid and dashed (red) curves]. Finally, the weights associated with $E^{\pm}_{NA}(\theta < 20°)$ are both on the order of one half and in principle both could be important for some purposes but $E^+_{\mathbf{k}}(x)$ corresponds to unoccupied states with positive energy.

So far we kept the magnetic coherence length fixed at a value $\xi=2.5$ in Figs. 6–9. Next we illustrate in Figs. 11 and 12 how the superconducting gap can further change when ξ is increased. One might reasonably expect that as the doping is reduced and the antiferromagnetic state in the cuprate phase diagram (which is also a Mott insulating state at $x=0$) is approached, the magnetic coherence length will increase. For simplicity we show here only results for $x=0.1$ and ξ increased to 10. Figure 11(a) gives the superconducting gap $\Delta_{sc}(\mathbf{k},T=0)$ at zero temperature as a function of momentum $\mathbf{k}$ in the BZ of the CuO_2 plane. Note the four large positive peaks with corresponding negative images which are well off the zone boundaries. The height of these peaks reaches ~4.3 meV while at the antinodal point the gap is only 1.2 meV. This is drastically different from the classical *d*-wave result represented by the lowest harmonic described earlier. The corresponding constant gap contours [light (black) lines] are given in Fig. 11(b) in the first quadrant of the CuO_2 plane

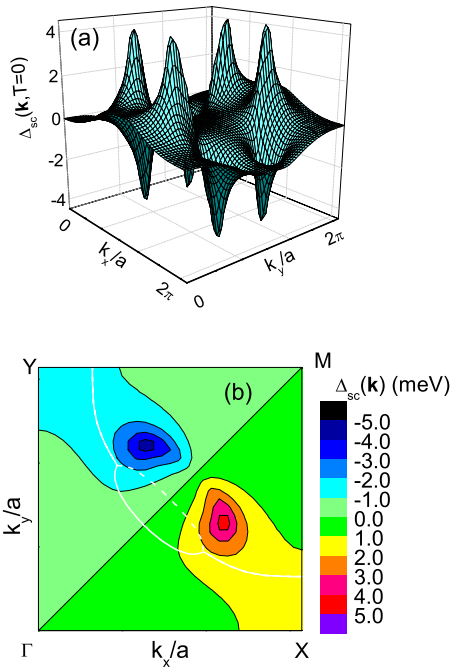

FIG. 11. (Color online) (a) Surface graph of the superconducting gap $\Delta_{sc}(\mathbf{k},T)$ as a function of momentum $\mathbf{k}$ in the two-dimensional BZ of the CuO_2 plane. The doping $x=0.1$ and the magnetic coherence length $\xi=10$. (b) Color plot of constant energies of the superconducting gap $\Delta_{sc}(\mathbf{k},T)$ in the first quadrant of the two-dimensional BZ of the CuO_2 plane.

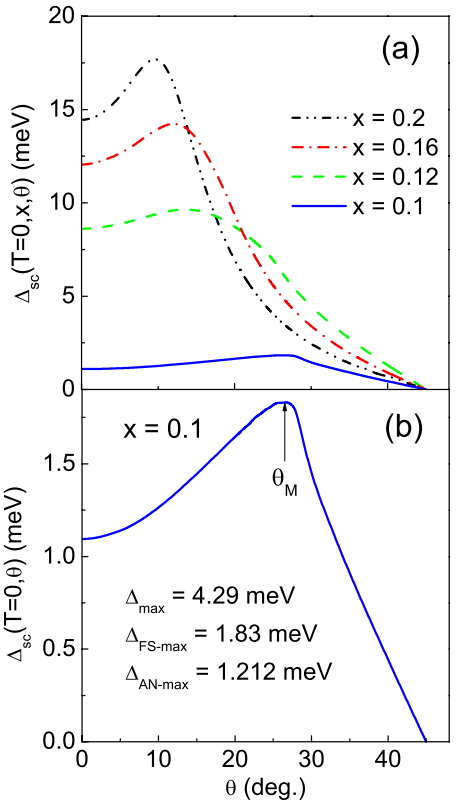

FIG. 12. (Color online) (a) The superconducting gap $\Delta_{sc}(T,x,\theta)$ for zero temperature as a function of the angle θ on the Fermi contour for various values of doping x as indicated in the figure. The magnetic coherence length $\xi=10$. (b) The same as above but for $x=0.1$ only. We find the gap to critical temperature ratio for the maximum gap in the BZ $2\Delta_{max}/(k_BT_c)=6.0$, for the maximum gap on the Fermi surface $2\Delta_{FS\text{-}max}/(k_BT_c)=2.55$, and for the maximum gap along the antinodal direction $2\Delta_{AN\text{-}max}/(k_BT_c)=1.7$.

BZ. We also show the Fermi contour as the heavy solid and dashed (white) lines. The superconducting gap is radically changed as compared with its momentum variation seen in the bottom right-hand frame of Fig. 6. Yet, only the magnetic coherence length has been altered in these two cases. This is further illustrated in Fig. 12. In Fig. 12(a) we show our results for the variation in the superconducting gap at $T=0$ on the Fermi contour for the four values of doping noted. All exhibit a nonmonotonic behavior with a peak away from the antinodal direction. This peak moves to larger angles as the doping is decreased. As the value of the critical temperature is reduced so is the amplitude of the gap. The case $x=0.1$ is further emphasized in Fig. 12(b) where we indicated the angle $\theta_M=26.5°$ at which the maximum on the Fermi contour occurs. At this angle $\Delta_{sc}=1.83$ meV which is 50% larger than its value at the BZ boundary (~ 1.2 meV). Both these values are much smaller than the maximum gap in the BZ equal to ~ 4.3 meV. As we saw in Fig. 11, this maximum occurs in the upper reduced AFBZ and has moved away from the antinodal direction toward the angle θ_{LP} indicated in Fig. 1. This angle marks the beginning of the Luttinger pocket. These features are a result of the choice of MMP model pairing potential which is highly peaked when the magnetic coherence length gets large as indicated schematically in Fig. 1. The (yellow) shaded circle is meant to represent the range in momentum space of $V_{\mathbf{k}'-\mathbf{k}=\mathbf{q}}$ about the hot spot defined as the crossing point between the Fermi contour and the AFBZ. Fermi-contour to Fermi-contour transitions through momentum transfer $\mathbf{q}=\mathbf{Q}$ equal to the commensurate magnetic vector (π,π) are in this case strongly favored by $V_{\mathbf{k}'-\mathbf{k}=\mathbf{q}}$. This leads to an increased contribution of higher order d-wave harmonics in the superconducting gap while it adjusts to the decreased effectiveness of the pairing potential away from momentum transfer $\mathbf{q}=\mathbf{Q}$. There is also a strong increase in the coupling parameter $g(x=0.2)$ with increasing values of ξ [see Fig. 3(b)]. An additional effect for the specific case considered here ($x=0.1$), is that there is also a pseudogap on the Fermi contour and this by itself is expected to reduce the effectiveness of such transitions in the pairing process as compared with the case of no pseudogap. Our detailed calculations show that the net result of all this is a superconducting gap that peaks at $\theta_M=26.5°$ in Fig. 12(b) with θ_M larger than $\theta_{AF}\sim 16.3°$. These same effects produce a nonmonotonic gap in all cases considered in Fig. 12(a). Clearly the YRZ model retains elements of competing order scenarios[21,22] where superconductivity competes for Fermi surface with pseudogap formation. Even for large values of the magnetic coherence length, however, our numerical results give nonzero superconducting gap values everywhere on the Fermi contour and, in particular, in the antinodal direction. Thus, we expect some temperature dependence of ARPES results in this direction in conflict with what was found by Kondo *et al.*[29]

V. SUMMARY AND CONCLUSIONS

The ansatz for the superconducting Green's function proposed by YRZ has had considerable success in providing a first qualitative and even semiqualitative understanding of the many properties of the underdoped cuprates previously considered anomalous. While the theory explicitly treats the formation of a pseudogap for dopings less than $x=x_{QCP}$ where x_{QCP} is the doping concentration at the quantum-critical point, the superconducting gap itself is treated only on the level of mean-field BCS and is taken to be a phenomenological parameter. Here we have addressed the question of how the superconducting gap itself is modified when the pseudogap is included in the normal-state electronic structure with attendant Fermi surface reconstruction. These represent profound changes in charge carrier dynamics as the Mott insulating state is approached. Because of this the superconducting properties of the underdoped cuprates are radically altered from the prediction based on ordinary *d*-wave BCS theory and so we might reasonably expect corresponding large changes in the behavior of the superconducting gap as well. Also the ARPES data of Kondo *et al.*[29] shows that the energy of nearest approach in the antinodal direction is temperature independent and, consequently, could be interpreted to mean that the superconducting gap is small in the antinodal region where it competes with a finite value of the pseudogap and large only on the Luttinger pocket. Here we consider both its structure in momentum space within the two-dimensional CuO_2 BZ and its evolution with temperature. The work proceeds through numerical solution of a generalized superconducting gap equation in which pseudogap formation is explicitly included. For the pairing potential the simplest possible form, based on a spin-fluctuation exchange mechanism is employed. In some calculations included for comparison, we also use a nearest-neighbor pairing potential. A fast Fourier transform technique is used to generate the solutions for the superconducting gap which are found to involve many higher-order harmonics beyond the lowest order. This is true even when no pseudogap is present and its structure in **k** space is strongly modified with changes in the magnetic coherence length and with increasing pseudogap. The superconducting gap does not vary with angle θ on the Fermi contour according to the simple BCS *d*-wave assumption $\sim\cos(2\theta)$ even near the nodal direction. In particular, for doping values around the QCP it shows concave upward behavior which becomes more linear in the highly underdoped regime. This effect is seen in some ARPES (Ref. 50) as well as FT-STS (Refs. 36, 48, and 49) experiments. As the magnetic coherence length is increased, as expected when the antiferromagnetic state is approached more closely, the superconducting gap acquires a strong nonmonotonic behavior as a function of θ and can have a maximum at an angle θ considerably before the antinodal direction is reached. But in all calculations the superconducting gap amplitude remains finite and significant in magnitude everywhere on the Fermi contour away from the Luttinger pocket where it competes directly with pseudogap formation and so might have been expected to be suppressed. Consequently, we find that there will always be some temperature dependence to the energy of nearest approach in the antinodal direction. This finding is in disagreement with some interpretation[7] of the data by Kondo *et al.*[29]

Another result is that the temperature dependence of the gap amplitude is altered from its classical mean-field value. Furthermore, the dimensionless ratio of zero-temperature gap to critical temperature is strongly affected by the pseudogap and varies considerably with doping. It is close to its canonical *d*-wave BCS value of 4.3 around optimal doping but increases particularly strongly for $x\leq 0.12$ rising to values beyond 6 and this implies that the superconducting dome for the gap differs from that for the critical temperature. Nevertheless, this change and others described above for the most part do not result in large qualitative changes in the predicted properties of the underdoped cuprates as compared with those based on the simpler ansatz of YRZ. In this sense, our work justifies this approach as a first attempt at understanding some of the anomalous features found in the underdoped cuprates. But more subtle effects such as noted above are missing. What becomes clear from our solutions, however, is that the coupling strength of the charge carriers to the spin fluctuations needs to increase as the doping is reduced toward the highly underdoped region of the superconducting dome. This result is consistent with a dominant spin-fluctuation pairing mechanism. It is the growth of the pseudogap which brings down the value of the critical temperature as the antiferromagnetic Mott insulating state is approached and not a reduction in pairing strength. The electronic structure simply evolves toward an insulating state which is unfavorable to superconductivity and, consequently, the value of the critical temperature goes to zero. A different choice of pairing potential leads to the same conclusion, i.e., the strength of the pairing must increase with decreasing doping.

ACKNOWLEDGMENTS

Research supported in part by the Natural Sciences and Engineering Research Council of Canada (NSERC) and by the Canadian Institute for Advanced Research (CIFAR). E.S. acknowledges support by the Austrian Research Fund (FWF), Vienna, under Contract No. P18551-N16.

*schachinger@itp.tu-graz.ac.at

[1] T. Timusk and B. Statt, Rep. Prog. Phys. **62**, 61 (1999).
[2] K.-Y. Yang, T. M. Rice, and F.-C. Zhang, Phys. Rev. B **73**, 174501 (2006).
[3] B. Valenzuela and E. Bascones, Phys. Rev. Lett. **98**, 227002 (2007).
[4] E. Illes, E. J. Nicol, and J. P. Carbotte, Phys. Rev. B **79**, 100505(R) (2009).

[5] K.-Y. Yang, H. B. Yang, P. D. Johnson, T. M. Rice, and F. C. Zhang, EPL **86**, 37002 (2009).
[6] J. P. F. LeBlanc, E. J. Nicol, and J. P. Carbotte, Phys. Rev. B **80**, 060505(R) (2009).
[7] J. P. F. LeBlanc, J. P. Carbotte, and E. J. Nicol, Phys. Rev. B **81**, 064504 (2010).
[8] J. P. Carbotte, K. A. G. Fisher, J. P. F. LeBlanc, and E. J. Nicol, Phys. Rev. B **81**, 014522 (2010).
[9] F. Marsiglio, R. Akis, and J. P. Carbotte, Phys. Rev. B **36**, 5245 (1987).
[10] B. Mitrović, C. R. Leavens, and J. P. Carbotte, Phys. Rev. B **21**, 5048 (1980).
[11] E. Schachinger, J. M. Daams, and J. P. Carbotte, Phys. Rev. B **22**, 3194 (1980).
[12] E. Schachinger, J. P. Carbotte, and D. Basov, Europhys. Lett. **54**, 380 (2001).
[13] E. Schachinger and J. P. Carbotte, Phys. Rev. B **62**, 9054 (2000).
[14] E. Schachinger, J. J. Tu, and J. P. Carbotte, Phys. Rev. B **67**, 214508 (2003).
[15] J. P. Carbotte, E. Schachinger, and J. Hwang, Phys. Rev. B **71**, 054506 (2005).
[16] J. Hwang, E. J. Nicol, T. Timusk, A. Knigavko, and J. P. Carbotte, Phys. Rev. Lett. **98**, 207002 (2007).
[17] J. Hwang, J. Yang, T. Timusk, S. G. Sharapov, J. P. Carbotte, D. A. Bonn, R. Liang, and W. N. Hardy, Phys. Rev. B **73**, 014508 (2006).
[18] H. K. Leung, J. P. Carbotte, D. W. Taylor, and C. R. Leavens, Can. J. Phys. **54**, 1585 (1976).
[19] P. G. Tomlinson and J. P. Carbotte, Phys. Rev. B **13**, 4738 (1976).
[20] H. K. Leung, J. P. Carbotte, and C. R. Leavens, J. Low Temp. Phys. **24**, 25 (1976).
[21] S. Chakravarty, R. B. Laughlin, D. K. Morr, and C. Nayak, Phys. Rev. B **63**, 094503 (2001).
[22] J.-X. Zhu, W. Kim, C. S. Ting, and J. P. Carbotte, Phys. Rev. Lett. **87**, 197001 (2001).
[23] J. Meng, G. Liu, W. Zhang, L. Zhao, H. Liu, X. Jia, D. Mu, S. Liu, X. Dong, J. Zhang, W. Lu, G. Wang, Y. Zhou, Y. Zhu, X. Wang, Z. Xu, C. Chen, and X. J. Zhou, Nature (London) **462**, 335 (2009).
[24] A. J. Millis, H. Monien, and D. Pines, Phys. Rev. B **42**, 167 (1990).
[25] C. O'Donovan and J. P. Carbotte, Phys. Rev. B **52**, 4568 (1995).
[26] C. O'Donovan and J. P. Carbotte, Physica C **252**, 87 (1995).
[27] D. Branch and J. P. Carbotte, Phys. Rev. B **52**, 603 (1995).
[28] C. O'Donovan and J. P. Carbotte, Phys. Rev. B **52**, 16208 (1995).
[29] T. Kondo, R. Khasanov, T. Takeuchi, J. Schmalian, and A. Kaminski, Nature (London) **457**, 296 (2009).
[30] M. Le Tacon, A. Sacuto, A. Georges, G. Kotliar, T. Gallais, D. Colson, and A. Forget, Nat. Phys. **2**, 537 (2006).
[31] W. Guyard, A. Sacuto, M. Cazayous, Y. Gallais, M. Le Tacon, D. Colson, and A. Forget, Phys. Rev. Lett. **101**, 097003 (2008).
[32] W. Guyard, M. Le Tacon, M. Cazayous, A. Sacuto, A. Georges, D. Colson, and A. Forget, Phys. Rev. B **77**, 024524 (2008).
[33] J. W. Lorama, K. A. Mirza, J. R. Cooper, and J. L. Tallin, J. Phys. Chem. Solids **59**, 2091 (1998).
[34] J. W. Loram, J. Luo, J. R. Cooper, W. Y. Liang, and J. L. Tallin, J. Phys. Chem. Solids **62**, 59 (2001).
[35] H.-B. Yang, J. D. Rameau, P. D. Johnson, T. Valla, A. Tsvelik, and G. D. Gu, Nature (London) **456**, 77 (2008).
[36] Y. Kohsaka, C. Taylor, P. Wahl, A. Schmidt, J. Lee, K. Fujita, J. W. Alldredge, K. McElroy, J. Lee, H. Eisaki, S. Uchida, D.-H. Lee, and J. C. Davis, Nature (London) **454**, 1072 (2008).
[37] W. Anukool, S. Barakat, C. Panagopoulos, and J. R. Cooper, Phys. Rev. B **80**, 024516 (2009).
[38] Y. J. Uemura, G. M. Luke, B. J. Sternlieb, J. H. Brewer, J. F. Carolan, W. N. Hardy, R. Kadono, J. R. Kempton, R. F. Kiefl, S. R. Kreitzman, P. Mulhern, T. M. Riseman, D. L. Williams, B. X. Yang, S. Uchida, H. Takagi, J. Gopalakrishnan, A. W. Sleight, M. A. Subramanian, C. L. Chien, M. Z. Cieplak, G. Xiao, V. Y. Lee, B. W. Statt, C. E. Stronach, W. J. Kossler, and X. H. Yu, Phys. Rev. Lett. **62**, 2317 (1989).
[39] A. Kanigel, M. R. Norman, M. Randeria, U. Chatterjee, S. Souma, A. Kaminski, H. M. Fretwell, S. Rosenkranz, M. Shi, T. Sato, T. Takahashi, Z. Z. Li, H. Raffy, K. Kadowaki, D. Hinks, L. Ozyuzer, and J. C. Campuzano, Nat. Phys. **2**, 447 (2006).
[40] A. Kanigel, U. Chatterjee, M. Randeria, M. R. Norman, S. Souma, M. Shi, Z. Z. Li, H. Raffy, and J. C. Campuzano, Phys. Rev. Lett. **99**, 157001 (2007).
[41] M. R. Norman, A. Kanigel, M. Randeria, U. Chatterjee, and J. C. Campuzano, Phys. Rev. B **76**, 174501 (2007).
[42] C. C. Homes, S. V. Dordevic, D. A. Bonn, R. Liang, and W. N. Hardy, Phys. Rev. B **69**, 024514 (2004).
[43] J. Hwang, T. Timusk, and G. P. Gu, J. Phys.: Condens. Matter **19**, 125208 (2007).
[44] J. Hwang, J. P. Carbotte, and T. Timusk, Phys. Rev. Lett. **100**, 177005 (2008).
[45] J. Hwang, J. Yang, J. P. Carbotte, and T. Timusk, J. Phys.: Condens. Matter **20**, 295215 (2008).
[46] J. Hwang, J. P. Carbotte, and T. Timusk, EPL **82**, 27002 (2008).
[47] E. Bascones and B. Valenzuela, Phys. Rev. B **77**, 024527 (2008).
[48] K. McElroy, R. W. Simmonds, J. E. Hoffman, D.-H. Lee, J. Orenstein, H. Eisaki, S. Uchida, and J. C. Davis, Nature (London) **422**, 592 (2003).
[49] T. Hanaguri, Y. Kohsaka, J. C. Davis, C. Lupien, I. Yamada, M. Azuma, M. Takano, K. Ohishi, M. Ono, and H. Takagi, Nat. Phys. **3**, 865 (2007).
[50] S. V. Borisenko, A. A. Kordyuk, T. K. Kim, S. Legner, K. A. Nenkov, M. Knupfer, M. S. Golden, J. Fink, H. Berger, and R. Follath, Phys. Rev. B **66**, 140509(R) (2002).
[51] K.-Y. Yang, W.-Q. Chen, T. M. Rice, and F.-C. Zhang, Phys. Rev. B **80**, 174505 (2009).
[52] T. Dahm, J. Erdmenger, K. Scharnberg, and C. T. Rieck, Phys. Rev. B **48**, 3896 (1993).
[53] E. Schachinger, J. P. Carbotte, and T. Timusk, EPL **86**, 67003 (2009).
[54] E. Schachinger, M. G. Greeson, and J. P. Carbotte, Phys. Rev. B **42**, 406 (1990).
[55] T. Dahm, Phys. Rev. B **61**, 6381 (2000).
[56] A. Pushp, C. V. Parker, A. N. Pasupathy, K. K. Gomes, S. Ono, J. Wen, Z. Xu, G. Gu, and A. Yazdani, Science **324**, 1689 (2009).
[57] U. Chatterjee, M. Shi, D. Ai, J. Zhao, A. Kanigel, S. Rosenkranz, H. Raffy, I. Z. Li, K. Kadowaki, D. G. Hinks, Z. J. Xu, J. S. Wen, G. Gu, C. T. Lin, H. Claus, M. R. Norman, M. Randeria, and J. C. Campuzano, Nat. Phys. **6**, 99 (2010).
[58] V. J. Emery and S. A. Kivelson, Nature (London) **374**, 434 (1995).
[59] Y. Wang, L. Li, and N. P. Ong, Phys. Rev. B **73**, 024510 (2006).